



HAL
open science

Plugging of Hollow Fiber Lumen by a gel: threshold operating conditions unraveled by simulations

Adriana Ferreira, Patrice Bacchin, Pierre Aimar, Philippe Carvin, Ana Hipólito, Micheline Abbas

► To cite this version:

Adriana Ferreira, Patrice Bacchin, Pierre Aimar, Philippe Carvin, Ana Hipólito, et al.. Plugging of Hollow Fiber Lumen by a gel: threshold operating conditions unraveled by simulations. *Chemical Engineering Science*, 2023, 278, pp.118903. 10.1016/j.ces.2023.118903 . hal-04188272

HAL Id: hal-04188272

<https://hal.science/hal-04188272>

Submitted on 25 Aug 2023

HAL is a multi-disciplinary open access archive for the deposit and dissemination of scientific research documents, whether they are published or not. The documents may come from teaching and research institutions in France or abroad, or from public or private research centers.

L'archive ouverte pluridisciplinaire **HAL**, est destinée au dépôt et à la diffusion de documents scientifiques de niveau recherche, publiés ou non, émanant des établissements d'enseignement et de recherche français ou étrangers, des laboratoires publics ou privés.

Plugging of Hollow Fiber Lumen by a gel : threshold operating conditions unraveled by simulations

ADRIANA FERREIRA^{a,b}, PATRICE BACCHIN^a, PIERRE AIMAR^a, PHILIPPE
CARVIN^b, ANA HIPÓLITO^b, AND MICHELINE ABBAS^a

^a*Laboratoire de Génie Chimique, Université de Toulouse, CNRS, INPT, UPS, Toulouse, France*

^b*Solvay, Research and Innovation Center of Lyon, Saint-Fons, France*

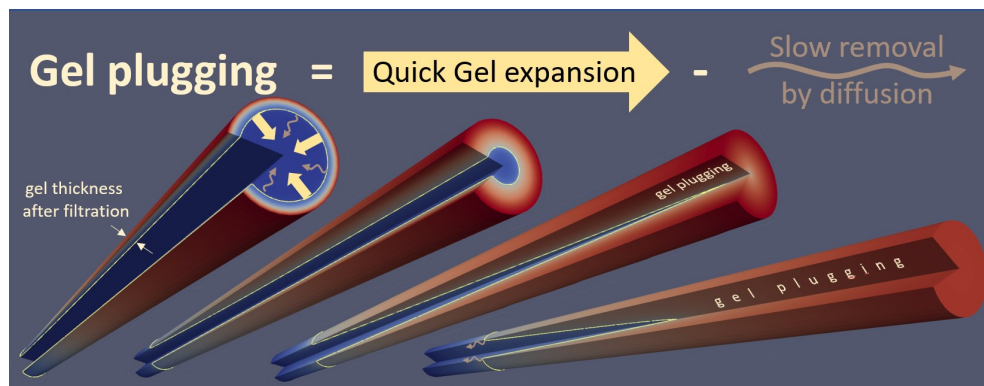
Abstract

Membrane processes may experience gel plugs that require specific cleaning steps. This paper demonstrates with simulations how these plugs can occur. A physical model is used to describe the particular diffusive behavior of gels. This model is implemented in an OpenFOAM CFD simulation code to describe the dynamics of the gel layers when filtration is stopped. During this step of relaxation, it is shown that the gel can expand and lead to a plug with characteristic times in the order of minutes. The plugging is favored by a quick gel expansion and by a slow diffusion removal. The operating conditions leading to the gel plugging are analyzed and threshold conditions are unraveled. General practical recommendations on the process control are drawn from these results.

Highlights (3 to 5 bullet points maximum 85 characters, including spaces, per bullet point)

- Plugging of a lumen by a gel is simulated during a relaxation when filtration stops
- The plugging is favored by a quick gel expansion and by a slow diffusion removal
- Severe fouling and irreversibly degree of the gel are conditions leading to plugging

Graphical abstract (readable at a size of 5 * 13 cm)



1 Introduction

In a number of situations, switching off the cross-flow or the driving pressure in a membrane filtration system may lead to unexpected consequences such as the blocking of the feed channels. Whether this sudden shut down is intentional at the end of a production session or unintentional because of a pressure or temperature peak has been detected or a particle has blocked the inlet lumen of a hollow fiber, the consequences are dramatic in terms of time and energy spent at cleaning the system until its process capacity has been restored. Whereas numerous experimental and numerical studies available in the literature provide quite a comprehensive understanding of the fouling phenomena, the dynamics of the mechanisms occurring right after the system has been turned off are far from being understood [1].

These phenomena certainly occur because the retentate in the channel cannot flow anymore. In most cases, this non-flowing matter has the form of a gel. It has been established that the way a colloidal gel was formed [2] has an impact on the cleaning efficiency afterwards. In waste water treatment for example, the gel formed by extracellular polymeric substances (EPS) can lead to clogging the feed channels [3]. The addition of calcium to alginate solutions, often used as models for EPS, can lead to irreversible fouling to such an extent that it plugs the lumen of the capillaries [4]. These mechanisms are linked to the properties of gels and to their propensity to relax and are thus strongly dependent on the interaction between particles forming the gels, hence on the electrolyte composition, pH ... [5], [6]. When filtering casein micelles, analysis of local concentration profiles via *in situ* SAXS suggested that gel swelling after pressure release was strongly temperature dependent [7].

Understanding these events is of theoretical but also technical importance. Unlike gravity-driven membrane reactors where the long time scales involved allow experimental measurements (like tomography) of the film evolution associated with filtration/relaxation strategies [8], the experimental techniques are scarce to investigate *in situ* and in real time what happens inside channels or thin fibers once the pressure difference or the cross-flow have been zeroed. One can find multiphase flow simulations combined to microfluidic experiments to have a better understanding of the mechanisms

of resuspension events during membrane backwashing of micrometric particles [9, 10, 11]. However, there are less studies investigating the same phenomena but for smaller particles or macromolecules. The rare simulations performed to describe the dynamics of relaxation of gel layers have been performed at a very local scale of a few thousands of particles. However, in membrane processes, fouling layers can contain millions of 10 nm particles per μm^2 of membranes area. Nevertheless, the time scale of gel relaxation can be very large and strongly depends on the physico-chemical properties [12], thus leading to difficulties to predict the fate of the fouling layers after the end of a filtration step. Numerical tools and physical models that allow capturing the phenomena at small scales are required to study the dynamics at the scale of the filtration process. In a previous work, we had developed an Eulerian model describing the sol-gel transition at the process scale, in which the physico-chemical and colloidal properties are accounted for via an osmotic pressure based approach (Π -based model). Its relevance at describing situations occurring in membrane systems has been shown in [13, 14]. The osmotic pressure is then the descriptor of local scale multi-body inter-particle interactions: its variations with the colloids volume fraction, $\Pi = f(\phi)$ can be seen as an equation of state for the colloidal suspension. It can be implemented in Eulerian equations for large scale simulations.

It is interesting to understand the way a gel has formed, in order to better predict its fate after the filtration. The formation of a gel results from a phase transition : the nature of surface interaction changes from repulsion (ensuring stability of the suspension) to attraction (leading to the gel). The relationship describing the osmotic pressure, $\Pi = f(\phi)$, is then modified by terms reflecting the attractive interactions. The model we have developed to depict the sol-gel phase transition of a dispersion [15] accounts for different gel reversibility degrees. The diffusion coefficient required in an Eulerian model can then be derived from the Π -based model via the generalized Stokes-Einstein equation. When the condition are getting close to the phase transition, the osmotic pressure variation versus the colloids concentration reaches nearly a plateau corresponding to the attractive forces balancing the dispersive forces. This quasi-plateau in the equation of state can be also interpreted as a dramatic decrease in the diffusion coefficient, reflecting the existence of an "arrested phase" during gel formation, that can be more or less irreversible, depending on the

colloidal interactions.

The purpose of the present work was to use the theoretical framework mentioned above and detailed in sections 2 and 3.3, in order to describe the formation of a gel and its subsequent relaxation once the cross-flow has been stopped and hence that the pressure difference between the retentate and permeate compartments has returned to zero. For the sake of model simplicity, we shall work in a cylindrical geometry, simulating a hollow fiber or tubular configuration and assume that the dynamics of stopping the cross-flow is fast compared to the one of relaxing the gel layers, as in an emergency shut-down or a head-blocking event in a hollow fiber bundle.

2 Π -based modeling of colloidal phases

The Π -based model relies on experimental or numerical data of the osmotic pressure as a function of the volume fraction. This property, that is considered as an equation of state for a colloidal dispersion, allows to account for the changes in the physical chemistry of a dispersion with its concentration [16, 13, 14]. In fig.1 a), a fit of experimental data for colloids [17] illustrates the different phases encountered when concentrating colloid :

- Ideal "gas like" phase when colloids are diluted and then free to move (Van't Hoff approximation)
- "liquid like" phase when colloids are close enough (and then concentrated enough) to interact (accounted for by the virial coefficients)
- "solid like" or gel phase when colloids form a cohesive phase mostly resulting from the percolation of attractive interactions (called usually gel and deposit in membrane science)

Let's note that in the solid phase, the Π -term should no more be called osmotic pressure (with its thermodynamic definition) but compressive yield stress (mechanical property) : the particles form a large network and the interactions between them become dominated by mechanical friction.

In this paper, we use the osmotic model specifically developed [15] to depict the phase transition. Knowing the osmotic pressure, it is possible to derive a collective diffusion coefficient (occurring in a concentration gradient) via a Stokes Einstein generalized law :

$$D(\phi) = D_0 \frac{1}{H(\phi)} \frac{V_p}{kT} \left(\frac{\partial \Pi}{\partial \phi} \right) \quad (1)$$

where Π stands for the osmotic pressure, V_p refers to the volume of a particle with radius, a ; $D_0 = \frac{kT}{6\pi\mu a}$ (where k and T correspond to the Boltzmann constant and temperature respectively) is the "ideal" diffusion coefficient, $H(\phi)$ is the Happel hindered settling coefficient [18], $H(\phi) = \frac{1}{K(\phi)} = \frac{6+4\phi^{\frac{5}{3}}}{6-9\phi^{\frac{1}{3}}+9\phi^{\frac{5}{3}}-6\phi^2}$. The Stokes Einstein generalized law can be extended to express the filtercake compaction by estimating the diffusivity of a cake from the compressive yield stress derivative [19].

An example of the collective diffusion coefficient obtained from eq. 1 is shown in Fig. 1b) as a function of the volume fraction. A minimum in the diffusion coefficient appears when the dispersion approaches the phase transition. The low diffusion coefficient corresponding to the plateau in the osmotic pressure curve in Fig 1a, $\Pi(\phi)$ is a hallmark of nearly arrested dynamics like colloidal gels or glasses [20, 21]. In regions where the colloidal concentration is close to critical value, the relative velocity of between phases becomes negligible, as the drag force associated with the osmotic pressure gradient decreases significantly, thus leading to a slowed dynamics [22, 23]. As previously shown [15], the minimum of the diffusion coefficient allows to describe the slow dynamics of relaxation when the concentration is lowered after a filtration. The value of ϕ for which the diffusion coefficient is minimum will be called a critical volume fraction later in this paper. This approach can be generalized to other types of dispersion undergoing a phase transition during filtration.

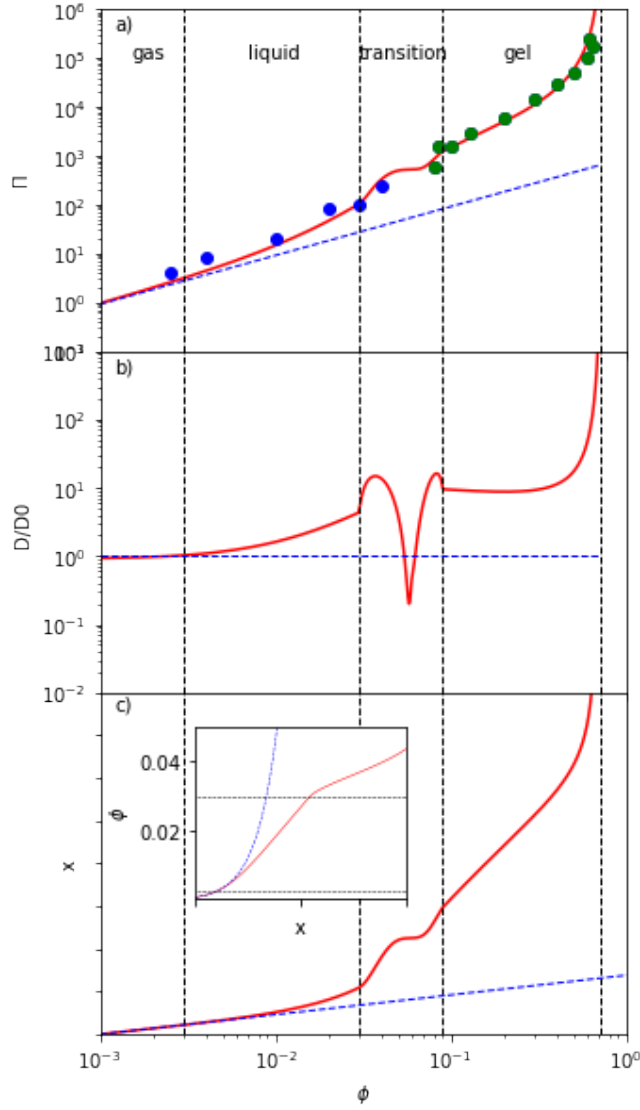


Figure 1: II-based modeling method : a) Experimental data from [17] and fitting of the osmotic pressure as a function of the volume fraction that leads to b) the estimation of the collective diffusion coefficient from Eq. 1. Finally, c), the concentration profile can be obtained by integration. The model allows to describe the different colloidal phases existing along the concentration range : the ideal or "gas like" phase described with a Van't Hoff law for osmotic pressure, a constant diffusion coefficient and an exponential concentration profile at the membrane -blue dashed lines-, a "liquid like" phase where colloids interacts but are still a dispersed sol and a phase transition leading to a cohesive phase (deposit or gel) for high concentration until the close packed volume fraction, ϕ_{cp} . In c) the concentration profile is a non conventionnal semilog plot of the distance as a function of the concentration but the inset displays the resulting conventional plot of the concentration profile.

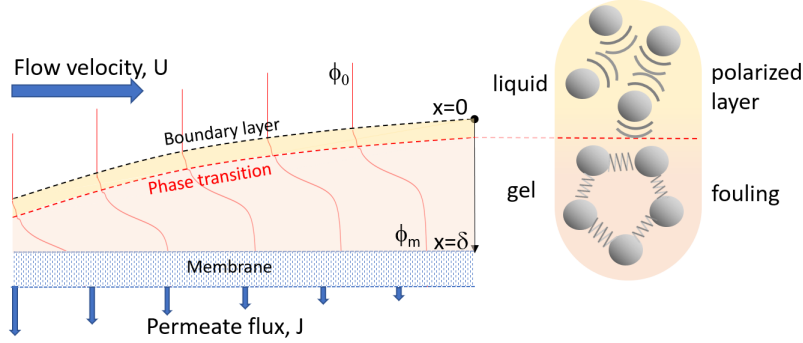


Figure 2: Scheme of the diffusive (or mass) boundary layer at the membrane surface consisting of a polarized layer and a gel layer. Collective diffusion describes this behavior by taking into account interparticle forces due to the repulsion (in the polarized layer), attraction (involved in sol/gel transition) and friction (in compacted layers). The particle-membrane interactions are neglected in this study.

The concentration profile in the layer near the membrane (Fig. 2) can be obtained by solving the mass balance in which the variation of the diffusion coefficient is given by equation 1. We assume a fully retentive membrane. We neglect the particle-membrane interactions. This assumption leads to consider that fouling is controlled by particle-particle interaction which is mainly the case during the filtration of concentrated dispersions leading to multilayers accumulation; in this case, the effect of first particle-membrane interaction are few important. We use the rectilinear coordinate x in the direction normal to the membrane, with $x = 0$ at the boundary layer limit (the border of the accumulation region) and $x = \delta$ at the membrane. This allows us to plot a unique solution, applicable for every filtration condition. At steady-state, the differential equation to be solved is:

$$J\phi - D(\phi) \left(\frac{\partial \phi}{\partial x} \right) = 0 \quad (2)$$

where J is the solvent permeation flux through the membrane **assumed to be constant along x** . When eq. 2 is integrated, the concentration profile $\phi(x)$ is obtained for every distance x with respect to the boundary layer limit where the concentration is equal to that of the bulk, ϕ_0 , according to:

$$x = \frac{1}{J} \int_{\phi_0}^{\phi(x)} D(\phi) \frac{d\phi}{\phi} \quad (3)$$

An example of the concentration profile, $\phi(x)$, corresponding to the diffusion coefficient in Fig 1b), is displayed in Fig. 1c). In the dilute range ("ideal" phase) close to the boundary layer limit, the profile follows an exponential growth associated with the constant diffusion coefficient. At higher concentration ("sol" phase in fig. 1b)), the increase in concentration becomes less significant as particles tend to repel each other, i.e. the colloids exhibit a higher osmotic pressure. Close to the phase transition a rapid increase (jump) in concentration takes place, indicating the formation of a denser phase. Once the denser phase has been formed, any further increase in concentration corresponds to a compaction of this dense layer up to the random close-packing volume fraction ϕ_{cp} . It has to be noted that the plotted concentration profile spans the widest possible range of concentrations (from ϕ_0 to ϕ_{cp}). In practice, the concentration profile is truncated at x corresponding to the boundary layer thickness δ which is controlled by the system hydrodynamics (axial flow), leading to different maximum concentration at the membrane, ϕ_m according to:

$$\frac{J\delta}{D_0} = \int_{\phi_0}^{\phi_m} \frac{D(\phi)}{D_0} \frac{d\phi}{\phi} \quad (4)$$

For ideal dispersions, $D(\phi) = D_0$, Eq. 4 simplifies into the well known film model, $J = \frac{D_0}{\delta} \ln(\frac{\phi_m}{\phi_0})$, plotted in dashed line in Fig.1c. The divergence between the solid and dashed lines in this figure can be ascribed to the effect of interfacial interactions on the particle distribution.

In this paper, this II-based modeling approach will be used to simulate the concentration profiles during accumulation (filtration mode) and relaxation (system switched off) steps for a "non-ideal" colloidal system such as the one depicted in Fig. 1b). Simulations will be performed in a 2D geometry representing a hollow fiber as explained in next section.

3 Numerical modelling

The filtration through a hollow fiber is considered, as outlined in figure 3. A suspension flow enters into the tube with a **parabolic velocity profile** (left side of the domain in figure 3) and prescribed pressure at the tube outlet. The boundary of the domain is a wall that mimics an idealized membrane. During the deposit build-up, a permeate flux (purified fluid) is allowed to pass through

the wall in the radial direction, whereas the colloids are considered to be fully retained (no particle flux through the wall). This leads to concentration polarization at the membrane whereas the concentration at the center of the fiber remains equal to the bulk concentration ϕ_0 . The filtration law is imposed at the membrane to account for permeability reduction due to fouling. A system shut down is simulated by equating the cross-flow and the filtration flux to zero. The domain boundaries are then considered impermeable to both the particles and the fluid. We then observe numerically the way the colloids accumulated at the membrane during the filtration step, now can diffuse back towards the axis of the fiber. The origin of time ($t=0$) in Figures 4 to 11 is taken when the system is switched off.

3.1 Operating conditions

The liquid phase consists of pure water, of density $\rho = 1000\text{kg}/\text{m}^3$ and viscosity $\mu = 10^{-3}\text{Pa}\cdot\text{s}$. The hollow fiber inner radius is taken to be $R = 0.4\text{mm}$. When the flow velocity across the fiber section at the entrance of the fiber U (used during the accumulations stage) is equal to $1.25 \times 10^{-2}\text{m}/\text{s}$, the flow Reynolds number $Re = \frac{\rho U(2R)}{\mu}$ is equal to 10. The colloidal particles are assumed to have a uniform radius, $a = 10\text{nm}$, leading to a diffusion coefficient in water at 25°C equal to $D_0 = \frac{k_B T}{6\pi\mu a} = 2.2 \times 10^{-11}\text{m}^2/\text{s}$. The other physico-chemical properties (surface charge, Hamaker constant, ...) are embedded in the Π -term (Fig. 1a). During the filtration stage in cross-flow conditions, the bulk volumetric concentration at the hollow fiber inlet ϕ_0 is set to a constant value between 1 and 4%. While the particles are advected by the flow, the competition between the transport by advection and diffusion is characterized by a Péclet number, of the form $Pe = \frac{J_0 R}{D_0}$, where J_0 is the permeate flux per unit area for the clean membrane (at the fiber entrance). Note that by construction here, the Péclet number based on the fiber radius and on the permeate flux at the clean membrane is constant, unlike other definitions that can be found in the literature where the Péclet is rather based on the boundary layer thickness which leads it to vary along the membrane length. The characteristic permeate flux J_0 is taken to be several orders of magnitude smaller than the main cross-flow velocity during the filtration, (for instance $J_0 = 5.5 \times 10^{-6}\text{m}/\text{s}$) leading to $Pe = 100$. Finally we consider that the tube length is $L = 40R$. Table 1 summarizes the

different dimensionless numbers used for this study.

Dimensionless number	Value
$\frac{J_0}{U}$	$3.3 \times 10^{-4}, 10^{-3}, 3 \times 10^{-3}$
$Re = \frac{\rho U(2R)}{\mu}$	10
$Pe = \frac{J_0 R}{D_0}$	100, 300, 900
a/R	2.5×10^{-5}
L/R	40

Table 1: Summary of the operating conditions written in dimensionless form.

3.2 Transport equations

The fluid equations of motion, i.e. continuity and momentum balance, are assumed to be weakly disturbed by the presence of colloidal particles. This presumes that the physical properties of the fluid (like the viscosity and Newtonian behavior of the fluid flow) are not modified at the macroscopic scale, which holds true as long as the concentration is relatively small. We will see at the end of this section that this assumption is satisfied during the accumulation stage as most of the flow regions are dilute, except in the thin polarized layer at the membrane, but not during the relaxation stage where the colloids can fill the entire section of the fiber. For this reason, the colloid relaxation is only considered in the absence of imposed cross-flow. Last, this assumption allows us to consider steady equations of the flow motion and unsteady transport equation for the colloidal phase, which reduces significantly the computational cost as the transient fluid flow equations would require very small time steps to be solved correctly.

The velocity and pressure fields during the accumulation state are set as following. Given that $L \gg R$, it can be shown that the steady-state solution of the velocity field in the $r - z$ plane follows eqs. 5 and 6

$$u_z(r, z) = -\frac{\partial p}{\partial z} \frac{R^2}{4\mu} \left[1 - \frac{r^2}{R^2} \right], \quad (5)$$

$$u_r(r, z) = \frac{\partial^2 p}{\partial z^2} \frac{R^2}{8\mu} r \left[1 - \frac{r^2}{2R^2} \right] \quad (6)$$

where u_r and u_z denote the velocity components in the radial and axial directions, respectively. The fluid viscosity μ is assumed to be constant. When accumulation is simulated, this assumption can have consequences on the kinetics of the gel layer formation. Considering concentration-dependence of the viscosity (in addition to the diffusion) induces a larger accumulated layer at the membrane. However the concentration profiles in the radial direction and the evolution of the boundary layer in the axial direction are relatively similar [14]. Also Park and Nagele have shown that neglecting the osmotic pressure effect at the membrane has a much stronger impact on the concentration polarization than neglecting the concentration-dependence of transport properties in particle ultra filtration. When the relaxation process is considered (the flow and permeate flux are turned off), this assumption would play a minor role on the initial condition used for the simulations but has no consequences on the dynamics in the simulations, as the mixture velocity is zero.

The pressure field p varies mainly in the axial direction. We further assume that the radial outflow velocity at the membrane surface is proportional to the effective pressure, i.e. the static pressure $p(z)$ of the fluid flow minus the local osmotic pressure $\Pi(\phi|_{r=R})$ that accounts for the colloid presence, $J(z) = L_p [p(z) - \Pi(\phi|_{r=R})]$. The coefficient L_p represents the effective membrane permeability the value of which is assumed to be constant. By means of a mass balance along the axial direction (averaged over the cross-section), the pressure should satisfy the following second order differential equation:

$$\frac{\partial^2 p}{\partial z^2} = \frac{16\mu L_p}{R^3} [p(r) - \Pi(\phi)], \quad (7)$$

The relation between the permeate velocity at the tube inlet and the membrane permeability via $J_0 = L_p \times p|_{z=0}$, assuming that the osmotic pressure at the inlet has a negligible contribution (dilute solution and absence of concentration polarization at the inlet), leading thus to the relationship $\frac{J}{J_0} = \frac{p(z) - \Pi(\phi|_{r=R})}{p(0)}$.

As for the colloidal particles, we apply a continuous description for their concentration field $\phi(r, z)$ that represents the local volume of particles averaged over a coarse-grained spatial scale

compared to the elementary volume corresponding to that scale. The equation of transport of the colloidal particles is similar to that usually used for a scalar, where material fluxes of convective and diffusive origin are both considered:

$$\frac{\partial \phi}{\partial t} = - \nabla \cdot [\phi \mathbf{u} - D(\phi) \nabla \phi] \quad (8)$$

The main difference with respect to a standard scalar transport equation lays in the dependence of the diffusion coefficient on particle concentration, $D(\phi)$, that can be described by the generalized Stokes-Einstein equation, eq. 1. As far as phase separation (spinodal decomposition) does not occur, equations 5, 6 and 8 capture the main features of the transport of colloidal particles by the flow inside a hollow fiber. During the relaxation stage, the velocity is set to zero, and the pressure in the fluid is constant all over the simulation domain. Therefore, transient effects on the particle transport, like spatial pressure homogenization, are not considered here.

3.3 Numerical setup and solver

Equations 7 and 8 were solved with the aid of the OpenFOAM (Open Field Operation and Manipulation) software, version Foundation 7, and they were run on a single node (36 cores) at the supercomputer Olympe at CALMIP center. The equation written with OpenFOAM formalism is given in the SI2 supplementary information. The OpenFOAM solver was customized to solve the transport equation (8) for the concentration field (ϕ) using equations 5 and 6 for the velocity field (\mathbf{u}). The solver includes the Π -based model of the diffusion coefficient (from eq. 1). The numerical solver is based on van Leer, Gauss, and Crank–Nicolson schemes for spatial discretization of the divergence and gradient terms, and for time advancement, respectively.

By means of axi-symmetry, the transport equations are solved in a 2D axi-symmetrical domain, with a mesh based on 400 grid points in the radial direction, 1 grid point in the azimuthal (angular) direction, and 2000 grid points in the axial direction (z-axis). The mesh illustrated in figure 3 is

regular, uniform in the axial direction but non-uniform in the radial direction, where the mesh elements are smaller near the wall, to better solve the stiff concentration gradients in that region (an expansion ratio of 0.1 was used in the radial direction). Different grid distributions were tested to verify that the results presented in this work are not significantly dependent on the mesh. As for the time step, we used $dt = 2 \times 10^{-4} T_a$, where $T_a = R/U$ is the advection time scale during the accumulation stage. During the relaxation, the time step was in such a way to respect the Fourier stability criteria ($dt < \Delta x_{min}^2 / (2D_0)$), where Δx_{min} denotes the smallest mesh size $\approx 6.2 \times 10^{-4} R$.

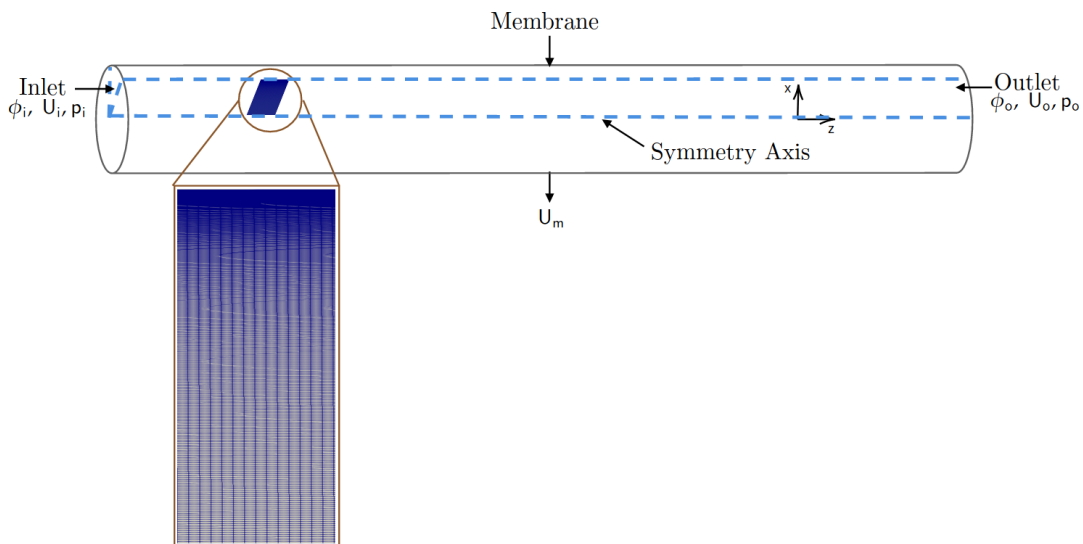


Figure 3: Configuration of the Cartesian 2D axis-symmetrical model in OpenFOAM (x -axis for the radial direction, y -axis for the angular directions, and z -axis for the axial direction).

As for the boundary conditions, the suspension concentration at the tube inlet is set to ϕ_0 , whereas the concentration gradient along the flow direction is set to zero at the outlet. At the wall, the zero particle flux is imposed in the radial direction. During the relaxation stage, this simply implies that the wall-normal concentration gradient $\frac{\partial \phi}{\partial x}|_{x=R} = 0$ as the flux is purely diffusive. However during the accumulation stage, the convection flux at the wall is different from zero, and thus we explicitly imposed at $x = R$ the following relation between the velocity and the

concentration as well as the concentration gradient:

$$\left[(u_r \phi) - D(\phi) \frac{\partial \phi}{\partial r} \right]_{r=R} = 0 \quad (9)$$

The permeate velocity ($u_r|_{r=R} = U_m$) (from eq. 5) and the subsequent concentration gradient obtained from eq. 9 were implemented using the library `swak4Foam`.

No theoretical solution exists for the full problem, with arbitrary concentration-dependent diffusion coefficient. However, when the diffusion coefficient is constant, the 2D problem (transport in a channel flow with permeable walls, the so-called Berman flow) has been solved theoretically at steady state by [24]. This solution has served as a first validation test for our numerical setup. Moreover, during the relaxation step, the accuracy of the code is validated by verifying the conservation of the mass in the volume of the fiber.

4 Results and discussion

During the simulations, the concentration field varying in space and time $\phi(r, z, t)$ can be recorded. To illustrate the simulation outcome, a 3D plot of the 2D- concentration contour of colloidal particles accumulated near the cylindrical fiber wall has been displayed in figure 4. Then figures 5 and 6 show the concentration field at different times during the relaxation of a fouling layer. In these figures, the concentration fields at the initial time correspond to the amount of colloids built up during the filtration of a suspension at $\phi_0 = 0.02$ and 0.04 , respectively.

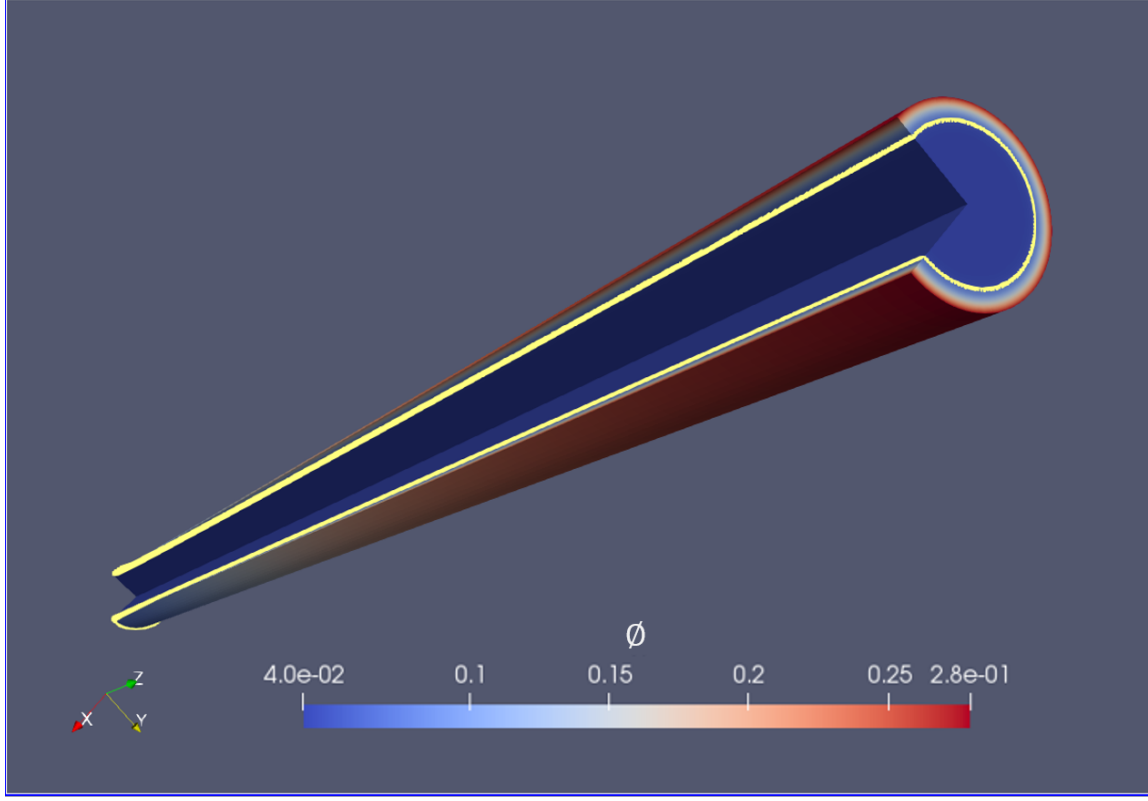


Figure 4: 3D plot of the concentrated layers inside the fiber for an injected concentration of $\phi_0 = 4 \times 10^{-2}$ after accumulation ($t = 0$). The yellow line denotes the limit of the gel phase, where the concentration is larger than $\phi_c = 0.06$.

The instantaneous space-averaged volume fraction is denoted as $\bar{\phi}(t)$. The total colloid volume accumulated in the lumen during the filtration stage, scaled by the total lumen volume leads to a space-average concentration $\overline{\phi_{acc}}(t)$

$$\overline{\phi_{acc}}(t) = \frac{\iiint_V \phi(t) r dr d\theta dz}{\pi R^2 L} \quad (10)$$

where θ denotes the angular coordinate. This quantity achieves a steady state after 15 seconds of filtration and remains constant during the relaxation stage, as a no-particle flux condition is imposed across all the fiber boundaries.

The simulations allow describing the temporal evolution of the regions filled with a gel, where the concentration exceeds the critical concentration ϕ_c . For instance in figures 4 and 6 the yellow lines indicate the contour level $\phi = \phi_c$. We define $\overline{\phi}_G$ as the total volume of colloidal particles in the form of a gel phase normalized by the hollow fiber volume as:

$$\overline{\phi}_G(t) = \frac{\iiint_{V|\phi>\phi_c} \phi(t) r dr d\theta dz}{\pi R^2 L} = \frac{m_{gel}(t)}{\rho_p \pi R^2 L} \quad (11)$$

that can be linked to the mass of gel, m_{gel} , in the hollow fiber for a given particle density, ρ_p . Similarly, the volume of the gel phase in the system is defined as the volume of the region filled with the gel over the hollow fiber volume:

$$\overline{V}_G(t) = \frac{\iiint_{V|\phi>\phi_c} r dr d\theta dz}{\pi R^2 L} \quad (12)$$

4.1 Occurrence of fiber plugging

Simulations of the accumulation and the relaxation steps have been performed for different concentrations of the feed suspension, ϕ_0 , and for different Péclet numbers, Pe . Figures 4 and 5 show the relaxation of the concentrated layers along the hollow fibers after filtration at Péclet number of 300 ($J_0 = 1.6 \times 10^{-5} m/s$) of suspensions of volume fraction 0.02 and 0.04 respectively. In the supplementary information SI3, the contours are given for the intermediate case of $\phi_0 = 0.03$ and the contours are represented with a full scale color map (the maximum of the scale is adapted) to have a better visualization of each concentration field. Figures 4 and 5 show two very different behaviors. For the more dilute conditions (Figure 4), the concentrated layers are progressively redispersed in the fiber. The volume of the gel, where concentration is above the critical concentration (yellow line), fades out and disappears after about 100 seconds. The relaxation dynamics is different when the fouling layer is the result of the filtration of a suspension at higher concentration (Figure 5). The initial gel layer expands over the entire section of the hollow fiber. This suggests a potential plugging of the lumen by the gel. The occurrence of this plugging depends on the operating conditions as shown in the following sections.

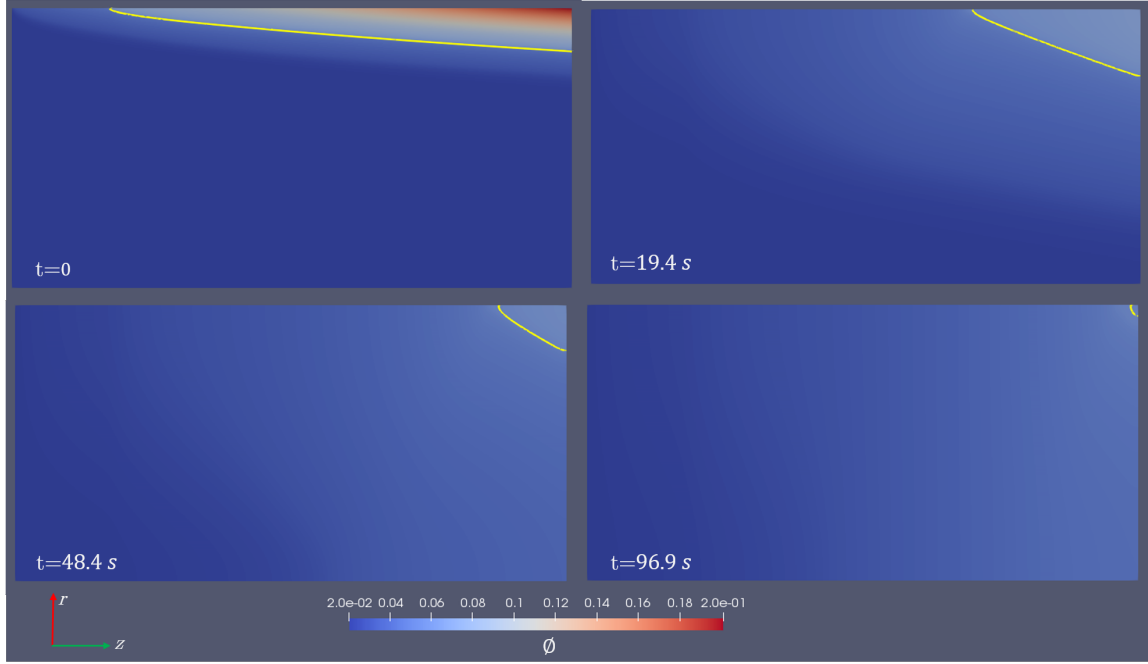


Figure 5: Contour plot of the concentrated layers inside the fiber for an injected concentration of $\phi_0 = 0.02$ after accumulation ($t = 0$) and during the relaxation times of $t = 19.4$ s, $t = 48.4$ s, and $t = 96.9$ s. The fiber length is scaled by a factor $1/20$ in the r -direction to ease the illustration of the concentration field. In each snapshot, the boundaries of each contour plot represent the membrane (top), the fiber center (bottom) the fiber inlet (left), and the fiber outlet (right). The yellow line denotes the limit of the gel phase, where the concentration is larger than $\phi_c = 0.06$.

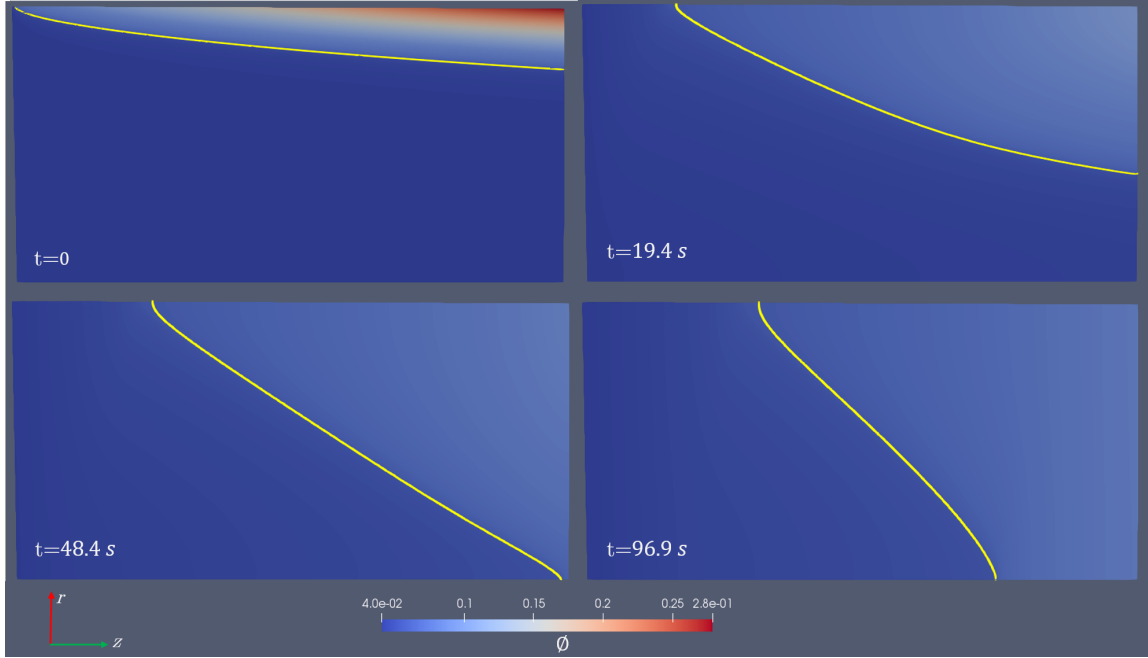


Figure 6: Idem figure 5 with $\phi_0 = 0.04$.

4.2 Effect of the feed volume fraction

Fig. 7 shows the time evolution of the volume fraction occupied by particles captured in a gel-like phase $\overline{\phi_G}$ and of the normalized fiber volume occupied by the gel $\overline{V_G}$ during the filtration ($t < 0$) and relaxation stages ($t > 0$) for various feed volume fraction, ϕ_0 , but with a constant filtration Péclet number, $Pe = 300$. During the accumulation stage, the quantity of formed gel reaches a plateau after a filtration time of the order of 10s. Upon relaxation, gel dispersion in the fiber depends on the feed volume fraction. At the lowest feed volume fraction, $\phi_0 = 0.01$, the volume of the gel phase is small and rapid gel dispersion is observed: it takes around 15s for the particles in the gel to be entirely dispersed in the fiber. At larger ϕ_0 , the time for its removal becomes longer, for instance around 1min for $\phi_0 = 0.02$.

If the concentration is further increased, we observe the relaxation of the gel layer in two stages, a trend that is especially clear when the signal of $\overline{V_G}$ is examined. For instance at $\phi_0 = 0.03$, at

the beginning of the relaxation stage, the gel volume slightly increases before eventually decreasing. The increase in the gel volume means that the polarized gel layer is expanding (see figure 7b). Afterwards, we observe a partial removal of the gel, for instance 35% during 100s after the filtration is stopped. This figure illustrates the gel expansion and its conjunction with the gel removal by diffusion during the relaxation step. For $\phi_0 = 0.04$, an increase in the amount of particles in the gel, $\overline{\phi}_G$ in Fig. 6a, is observed despite the fiber being closed to mass exchange with the exterior. It suggests that additional colloids are incorporated in the gel phase. It has to be noted that the expansion in the volume, \overline{V}_G , is also more pronounced compared to $\phi_0 = 0.03$. Thus there is no gel removal during the simulation time (100s).

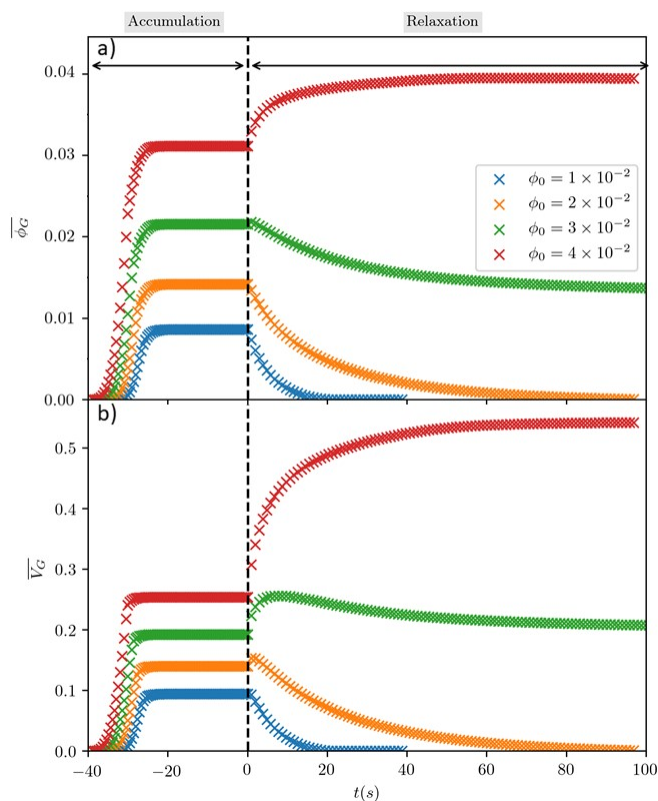


Figure 7: Evolution in time of a) $\overline{\phi}_G$, the volume fraction of particles captured in the form of gel-like phase b) \overline{V}_G , the volume of the gel during the accumulation and relaxation stages for different ϕ_0 .

The onset of the plugging of the hollow fiber can be tracked by monitoring the volume fraction ϕ at the fiber exit, i.e. at the point $r = 0$ and $z = L$. We consider that plugging occurs when the volume fraction ϕ at this position is equal to or larger than ϕ_c . Figure 7 shows the time evolution of $\phi(r = 0, z = L, t)$ at the fiber center versus time. This figure suggests that the fiber is plugged after 50s for $\phi_0 = 0.04$: indeed, the concentration increases up to the critical value leading to gel formation. Note that the sol/gel transition is marked by a steep increase of ϕ as the colloids are in metastable state in regions where the concentration range is close to phase the transition. For $\phi_0 = 0.03$, the global volume fraction of particles captured in a gel-like phase $\overline{\phi_G}$ decreases with time (as suggested by figure 7), but the volume fraction at the fiber center increases gradually to form a plug after around 3 min (inset of figure 8). It means that, during the mild increase of the concentration at the fiber center (before the sudden jump), there is a slow diffusion of the gel content towards the retentate phase. Eventually, the volume fraction of colloids remaining in the gel phase is still higher than the critical concentration whereas the volume fraction of colloids in the retentate phase has increased to such an extent that it overcomes the critical concentration: at the end, the whole fiber cross section is filled with a gel phase. The 2D contour (supplementary information 3) shows that at the end of the relaxation the gel occupies 21 % of the volume for a feed volume fraction, $\phi_0 = 0.03$, whereas the gel occupies 52% after the relaxation for the $\phi_0 = 0.04$ case.

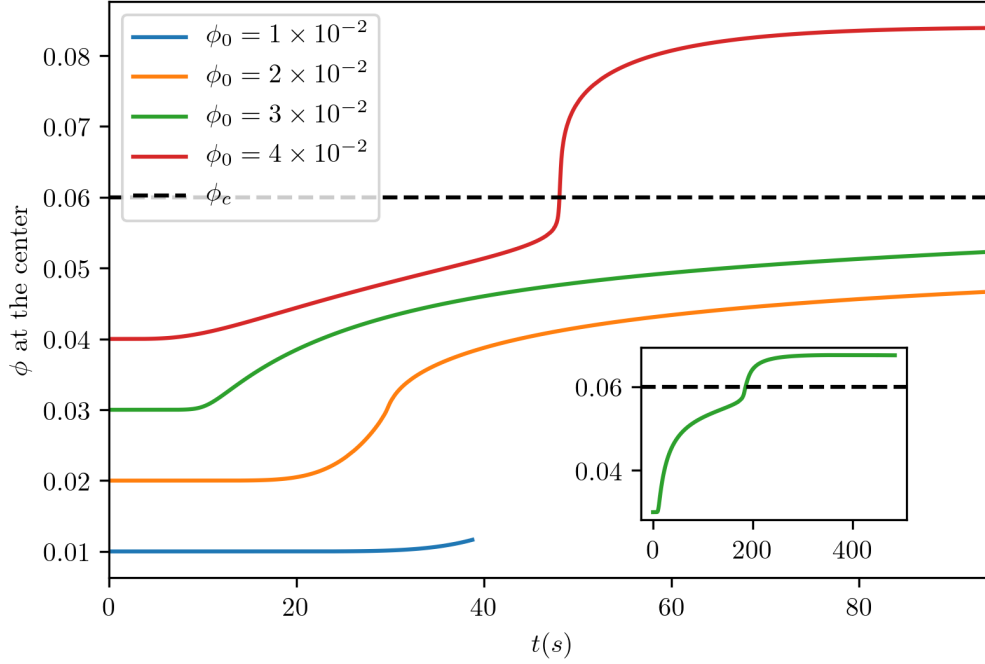


Figure 8: Time evolution of the colloid volume fraction $\phi(r = 0, z = L, t)$ during the relaxation stage. The inset gives the evolution for a longer time when $\phi_0=0.03$. The dashed line represents ϕ_c (the critical concentration). With time, the concentration in the center can reach the critical value leading to complete fiber plugging: this occurs when filtration is performed at $\phi_0 = 0.03$ and 0.04 .

Fig. 9 shows the radial concentration profile at the exit of the hollow fiber, $\phi(r, z = L)$ at different instants during the relaxation stage. The steep concentration variation corresponds to sol/gel phase transition. This figure illustrates the shift of the sol/gel front towards the hollow fiber center (from large to small r), associated with gel expansion. For the case $\phi_0 = 0.04$, the concentration jump reaches the center of the hollow fiber, leading to the fiber plugging by the gel, between 40 and 50s, which corresponds to the time range at which a concentration jump is observed on the red line of Fig. 8. From both figures, we thus conclude that the invasion of the fiber by the gel is captured by the sudden increase in the signal of the concentration at the fiber center $\phi(r = 0, z = L, t)$.

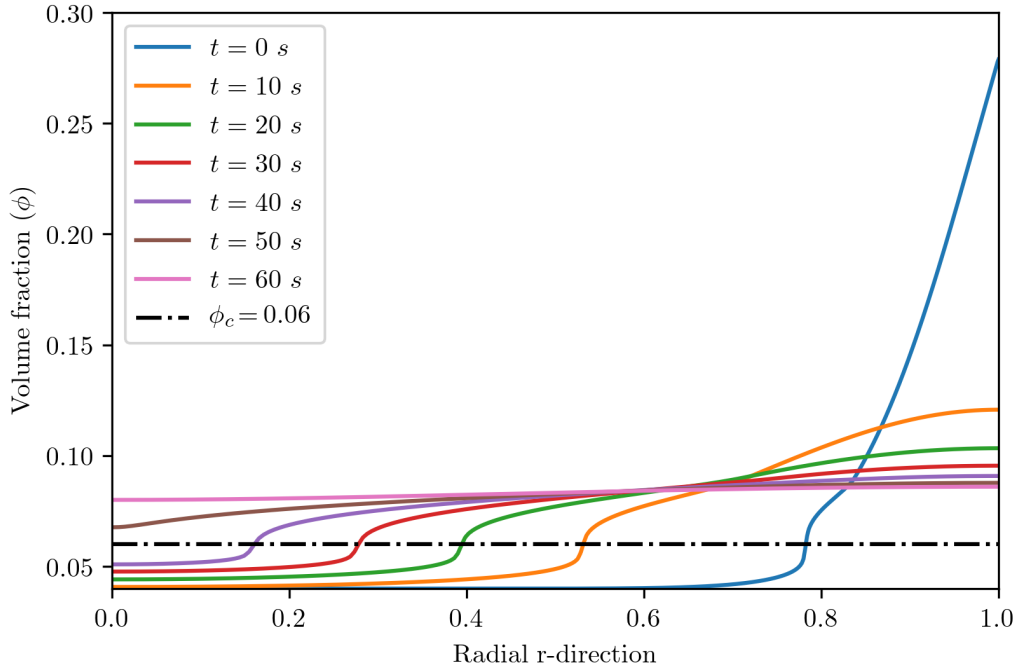


Figure 9: Radial profiles at the fiber outlet for the relaxation times of 0, 10, 20, 30, 40, 50, and 60s (from right to left) for $\phi_0 = 0.04$. The radial direction was scaled by the fiber radius: 0 and 1 correspond to the fiber center and membrane respectively.

4.3 Effect of the permeate flow during the accumulation stage

To investigate the impact of the filtration conditions during the accumulation stage on the plug formation, we performed simulations at various Péclet numbers (based on the permeate velocity, fiber radius and diffusion coefficient D_0). We show that both the Péclet number and the bulk volume fraction influence the quantity of gel accumulated in a given time, and thus the possibility of fiber plugging during the relaxation. The Péclet number Pe_r was varied between 100 and 900 and the volume fraction of the feed suspension ϕ_0 was varied between 0.01 and 0.04. Figure 10 illustrates the impact of the Péclet number on the time evolution of $\overline{\phi_G}$ during both the accumulation and relaxation stages for $\phi_0 = 0.04$ (the most concentrated case in this study). Increasing the Péclet number results in larger amount of particles trapped in the gel phase during the accumulation stage,

where steady state is reached after few seconds. During the relaxation stage, the curves of $\overline{\phi_G}$ suggest that when filtration was performed at $Pe_r = 100$, the retained particles in the form of a gel were not sufficient to expand and block the fiber. On the contrary, at $Pe_r = 300$ and 900 , $\overline{\phi_G}$ increases at the onset of the relaxation stage (more noticeably for $Pe_r = 900$), indicating the occurrence of additional incorporation of dispersed particles in the gel during gel expansion (as explained in the previous section). This analysis is supported by figure 11 that displays $\phi(r = 0, z = L, t)$ during the relaxation step. When the concentration at the fiber center exceeds the critical concentration ϕ_c , we consider that fiber plugging can potentially occur. This figure suggests that fiber plugging occurs after $28s$ (resp. $46s$) when $Pe_r = 900$ (resp. 300): the larger the Péclet number, the smaller is the time required to reach fiber plugging. These tests illustrate the importance of choosing a convenient set of operating conditions in order to avoid fiber plugging. If the concentration is relatively large, we can avoid plugging by decreasing the filtration velocity.

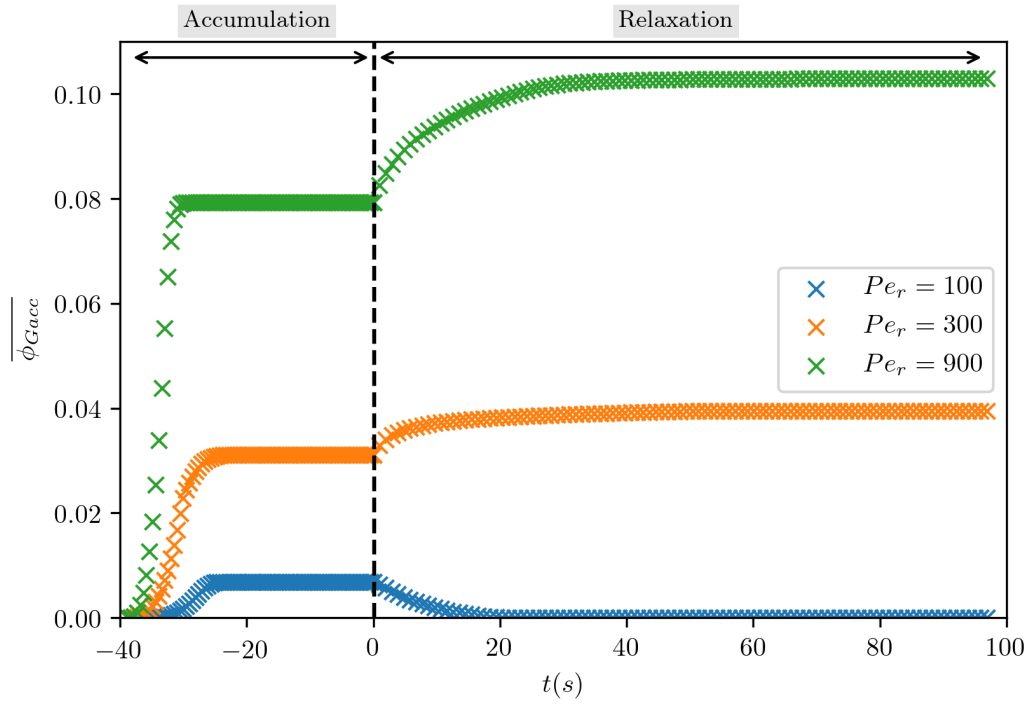


Figure 10: Volume of the particles in the gel during the accumulation and relaxation stages for a $\phi_0 = 0.04$, for different filtration conditions during the accumulation stage.

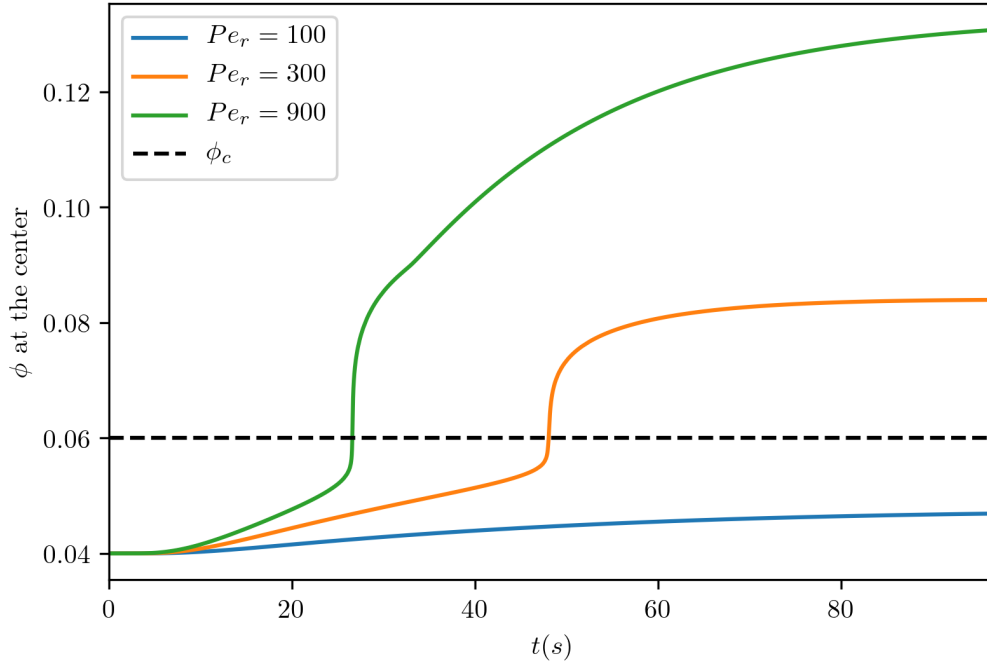


Figure 11: Volume fraction (ϕ) at the fiber center during relaxation for different filtration conditions during the accumulation stage for $\phi_0 = 0.04$.

4.4 Discussion and derived recommendations to avoid gel plugging

Our simulations show that two mechanisms happen during the relaxation of concentrated layers as sketched in the graphical abstract :

- a spatial expansion of the gel which was initially compressed on the membrane
- a redispersion of the colloidal particles from the gel by diffusion towards the liquid phase filling the rest of the lumen

Gel plugging occurs when the gel layers formed at the inner surface of the hollow fibers expand (predominantly in the radial direction) and reach the center of the fiber before eventual removal of the particles from the gel by diffusion.

To define the conditions leading to plugging, a phase diagram that indicates if the plugging occurs during relaxation according to the operating conditions during the accumulation step is plotted in Figure 12. For a feed concentration of 0.01, no plugging was observed whatever the Péclet number, whereas for higher feed concentrations, plugging is observed when the filtration Péclet number increases. In the cases where the inlet concentration was 0.03 and 0.04, no plugging was observed for a Péclet number of 100. This is mainly because at this Péclet number, the amount built-up is not sufficient to form a gel over the whole section of the hollow fiber. Figure 12 allows to appreciate that the gel plugging forms for conditions of filtration with high volume fraction and high permeation flux. As more fouling occurs during the accumulation stage, the risk of gel plugging increases and may occur more quickly after filtration has stopped.

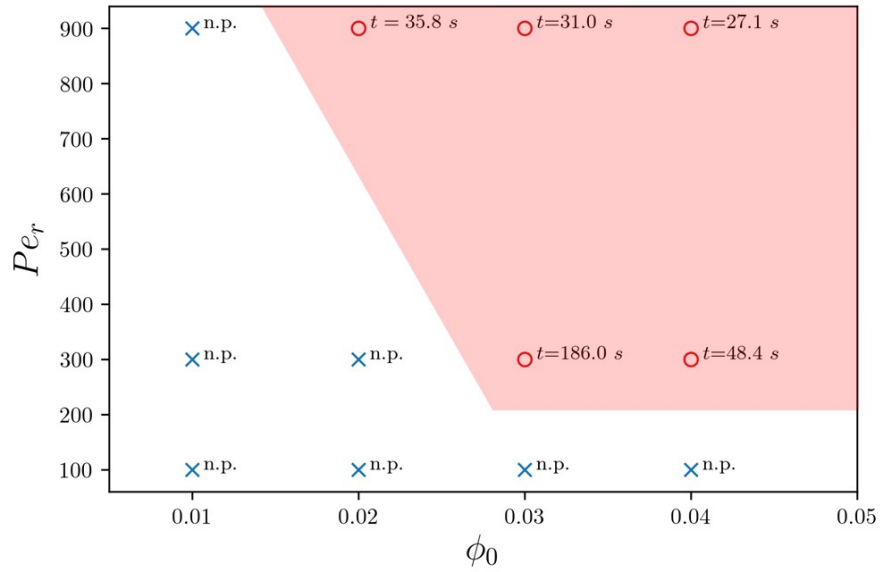


Figure 12: Impact of feed concentration (ϕ_0) and filtration conditions (Pe_r) on the fiber plugging. The blue crosses and red crosses indicate respectively that no plugging is observed (n.p.) or fiber plugging occurs after a numerically measured relaxation time. A colored area is added on the top of the diagram to indicate qualitatively the range of operating conditions that lead to fiber plugging.

To summarize, the gel plugging is thus favored :

- when the quantity of the gel and its compression at the membrane surface are important : it will act as a "compressed gel reservoir" that leads to a rapid spatial expansion
- when the gel is weakly reversible : it will lead to a slow removal by diffusion

The latter depends on the variation in the diffusion coefficient close to the phase transition point (Figure 1b). This parameter of the model discussed in a previous paper [15] can be linked to the temperature and to the inter-particle interaction that determine the ability to relax [22]. In a study of gel formation in hollow fibers with alginate (used as a model of EPS) [4], it has been shown that the addition of calcium that leads to irreversible gels can plug the lumen of the capillaries. The observation of gel plugging was also favored by high permeation fluxes. Our simulation data can explain the effects of these two parameters (permeate flux and gel irreversibility) on the plugging via the interplay between the characteristic times of the gel expansion (induced by the gel mechanical forces reflected in our model by the "diffusion coefficient" above the phase transition) and of the gel redispersion (by diffusion across the phase transition slowed down by the minimum of diffusion sketched in Fig. 1b).

Let's point out that the redispersion of the gel by diffusion is also dependent on the interfacial area between the gel and the solution. However, due to the cylindrical geometry of the hollow fiber, the interfacial area between the gel and the solution, where the redispersion occurs, is reduced as the gel expands toward the center. The gel/solution area is initially, when the gel is compressed at the membrane surface (Fig. 3), in the range of $2\pi RL = 40mm^2$ but is reduced to $\pi R^2 = 0.5mm^2$ when a plug is formed on the membrane section (Fig. 12). This drastic drop in gel/solution interfacial area reduces the kinetics of the gel removal by diffusion as soon as the gel plug is formed.

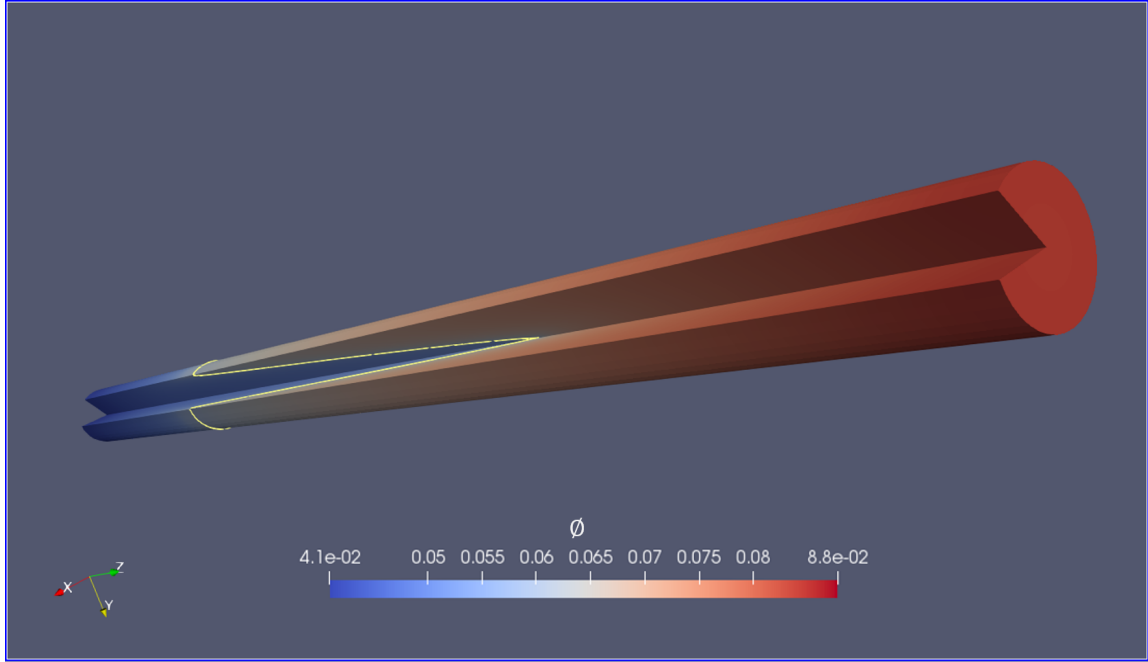


Figure 13: 3D representation of the gel plugging after a filtration made for a $\phi_0 = 0.04$ and à Péclet of 300 after a time of 100s. By comparing with the Fig. 3, at the beginning of the relaxation, it can be seen that the gel/dispersion area is reduced when the gel occupies the whole section of the hollow fiber that in turn leads to a drastic reduction of the gel removal.

Although the model is not validated by experimental data, qualitative practical recommendations can be drawn from these results.

- Avoid filtration conditions leading to severe fouling : as it exists critical conditions for the formation of gel during filtration [25, 26, 13], there is threshold conditions of filtration operating conditions that can lead to the bore plugging during the shut down of the filtration system (Figure 10) : the relaxation of the gel can lead to a blockage of the fiber lumen. It is well known that intensive filtration conditions lead to severe fouling. We show here that this can also lead to a complete plugging of the fibers by a gel.
- Never totally stop the cross flow in filtration rig after a controlled or unexpected system shut down : in the absence of an axial flow after the filtration, the expansion of the concentrated layers can lead to the formation of a plug on the whole section of the fibers sometimes in

few seconds. A gentle axial flow after the accumulation step can avoid the formation of gel plugging. Simulations can show this effect but there are not presented here as a quantitative simulation is not possible without taking into account the specific rheology of the concentrated phase (this was not necessary during the relaxation as only diffusion occurs)

- When working with modules with several hollow fibers or tubes in parallel, avoid fluctuations of axial flow rate. Preferential flows may lead to a higher flow and in turn more severe fouling in some fibers. If during the operation, the total flow rate fluctuates leading to a lower axial fiber in fibers with severe fouling, the relaxation of the accumulated layers can also lead to lumen plugging. Such phenomena are sometimes observed in industry during the filtration of a highly concentrated dispersion (fermentation broth, dairy products) in multi-channel tubular membranes.

5 Conclusions

Simulations of gel layer relaxation (after a filtration system has been switched off) have been performed in a cylindrical geometry, with an osmotic pressure based model accounting for the sol/gel phase transition. When the pressure and cross-flow are suddenly switched off, the simulations describe a rapid gel expansion and a progressive gel diffusion towards the retentate remaining within the lumen. Above the thresholds defined in the paper, this gel expansion can lead to complete plugging of the hollow fibers at time scales of about ten seconds or minutes depending on operating conditions. This plug occurs when the layers originally built up on the inner surface of the hollow fiber reach the fiber center. A plug is formed if the amount of retentate remaining in the lumen is not sufficient to disperse (by diffusion) the amount of colloids trapped in the gel phase, so that the final concentration falls below the critical concentration. This numerical work leads to practical recommendations : a cleaning step or a rinsing step must shortly follow the filtration step to prevent the gel from jamming the bore of the fiber. Keeping a cross flow, even low, to eliminate the layers of concentrate before their expansion is highly recommended.

6 Acknowledgment

Computational resources were provided by the computing meso-centre CALMIP under project no. P1002.

7 Nomenclature

ϕ	volume fraction field	
ϕ_0	bulk volume fraction	
ϕ_c	critical volume fraction sol/gel phase transition	
$\Pi(\phi)$	Osmotic pressure	[Pa]
ρ	fluid density	[kg.m ⁻³]
μ	fluid viscosity	[Pa.s]
a	particle radius	[m]
D_0	particle thermal diffusion from Stokes-Einstein relation	[m ² .s ⁻¹]
$D(\phi)$	particle collective diffusion	[m ² .s ⁻¹]
$H(\phi)$	Happel function	
$K(\phi)$	Sedimentation coefficient	
k_B	Boltzmann constant = $1.38064852 \times 10^{-23}$	[m ² .kg.s ⁻² .K ⁻¹]
L	fiber length	[m]
L_p	hydraulic permeability of the membrane	[(s.m ²).kg ⁻¹]
p	pressure field	[Pa]
r	radial direction	[m]
Pe_r	Péclet number based on the permeate velocity	
R	fiber diameter	[m]
Re	Reynolds number	
T	temperature	[K]
U_z	tangential velocity field	[m.s ⁻¹]
U_r	radial velocity field	[m.s ⁻¹]
V_p	particle volume	[m ³]
z	tangential direction	[m]

References

- [1] Z. Wang, J. Ma, C. Y. Tang, K. Kimura, Q. Wang, and X. Han. Membrane cleaning in membrane bioreactors: a review. *J. Memb. Sci.*, 468:276–307, 2014.

- [2] X. M. Wang and T. D. Waite. Role of gelling soluble and colloidal microbial products in membrane fouling. *Env. Sci. & Technol.*, 43(24):9341–9347, 2009. PMID: 20000527.
- [3] T. Zsirai, P. Buzatu, P. Aerts, and S. Judd. Efficacy of relaxation, backflushing, chemical cleaning and clogging removal for an immersed hollow fibre membrane bioreactor. *Water Res.*, 46(14):4499 – 4507, 2012.
- [4] Van de Ven W.J.C., van’t Sant K., Pünt I.G.M., Zwijnenburg A., Kemperman A.J.B., W.G.J. Van der Meer, and M. Wessling. Hollow fiber dead-end ultrafiltration: Influence of ionic environment on filtration of alginates. *J. Memb. Sci.*, 308(1-2):218–229, 2008.
- [5] E. Del Gado and W. Kob. Structure and relaxation dynamics of a colloidal gel. *Europhys. Lett.*, 72(6):1032–1038, 2005.
- [6] M. Doi. Gel dynamics. *J. Phys. Soc. Japan*, 78(5):052001, 2009.
- [7] F. Doudiès, M. Loginov, N. Hengl, M. Karrouch, N. Leconte, F. Garnier-Lambrouin, J. Pérez, F. Pignon, and G. Gésan-Guiziou. Build-up and relaxation of membrane fouling deposits produced during crossflow ultrafiltration of casein micelle dispersions at 12° c and 42° c probed by in situ saxs. *J. Memb. Sci.*, 618:118700, 2021.
- [8] L. Fortunato, L. Ranieri, V. Naddeo, and T. Leiknes. Fouling control in a gravity-driven membrane (gdm) bioreactor treating primary wastewater by using relaxation and/or air scouring. *J. Memb. Sci.*, 610:118261, 2020.
- [9] J. Lohaus, F. Stockmeier, P. Surray, J. Lölsberg, and M. Wessling. What are the microscopic events during membrane backwashing? *J. Memb. Sci.*, 602:117886, 2020.
- [10] A. Lüken, J. Linkhorst, R. Fröhlingdorf, L. Lippert, D. Rommel, L. De Laporte, and M. Wessling. Unravelling colloid filter cake motions in membrane cleaning procedures. *Sci. Rep.*, 10(1):20043, November 2020.
- [11] Z. B Sendekie and P. Bacchin. Colloidal jamming dynamics in microchannel bottlenecks. *Langmuir*, 32(6):1478–1488, 2016.

- [12] T. R. Kirkpatrick and D. Thirumalai. Colloquium: Random first order transition theory concepts in biology and physics. *Rev. Mod. Phys.*, 87:183–209, 3 2015.
- [13] P. Bacchin, B. Espinasse, Y. Bessiere, D. F. Fletcher, and P. Aimar. Numerical simulation of colloidal dispersion filtration: description of critical flux and comparison with experimental results. *Desalination*, 192(1-3):74–81, 2006.
- [14] Gun Woo Park and Gerhard Nägele. Modeling cross-flow ultrafiltration of permeable particle dispersions. *The Journal of Chemical Physics*, 153(20):204110, 2020.
- [15] A. Ferreira, M. Abbas, P. Carvin, and P. Bacchin. Colloid dynamics near phase transition: a model for the relaxation of concentrated layers. *Colloid Surf. A-Physicochem. Eng. Asp.*, page 128222, 2022.
- [16] Y. Bessiere, D. F. Fletcher, and P. Bacchin. Numerical simulation of colloid dead-end filtration: Effect of membrane characteristics and operating conditions on matter accumulation. *J. Memb. Sci.*, 313(1):52 – 59, 2008.
- [17] J. Chang, P. Lesieur, M. Delsanti, L. Belloni, C. Bonnet-Gonnet, and B. Cabane. Structural and thermodynamic properties of charged silica dispersions. *J. Phys. Chem.*, 99(43):15993–16001, 1995.
- [18] J. Happel. Viscous flow in multiparticle systems: slow motion of fluids relative to beds of spherical particles. *AIChE journal*, 4(2):197–201, 1958.
- [19] J. D. Sherwood. Initial and final stages of compressible filtercake compaction. *AIChE J.*, 43(6):1488–1493, 1997.
- [20] V. Trappe and P. Sandkühler. Colloidal gels—low-density disordered solid-like states. *Curr. Opin. Coll. Int. Sci.*, 8(6):494 – 500, 2004.
- [21] L. C. Johnson and R. N. Zia. Phase mechanics of colloidal gels: osmotic pressure drives non-equilibrium phase separation. *Soft Matter*, 17(14):3784–3797, 2021.

- [22] A. Di Biasio. Relaxation phenomena in sol–gel transition. *Colloid Surf. A-Physicochem. Eng. Asp.*, 140(1):279–287, 1998.
- [23] L. Cipelletti and L. Ramos. Slow dynamics in glassy soft matter. *J. Phys.: Cond. Matter*, 17(6):R253, 2005.
- [24] P. Haldenwang, P. Guichardon, G. Chiavassa, and N. Ibaseta. Exact solution to mass transfer in berman flow: Application to concentration polarization combined with osmosis in crossflow membrane filtration. *Int. J. Heat Mass Transfer*, 53(19-20):3898–3904, 2010.
- [25] P. Bacchin, B. Espinasse, and P. Aimar. Distributions of critical flux: modelling, experimental analysis and consequences for cross-flow membrane filtration. *J. Memb. Sci.*, 250(1-2):223–234, 2005.
- [26] P. Bacchin, P. Aimar, and R. W. Field. Critical and sustainable fluxes: theory, experiments and applications. *J. Memb. Sci.*, 281(1-2):42–69, 2006.

8 Supplementary information

8.1 SI1: Validation of the transport equations

The numerical transient solution of the transport equations was validated in a configuration inspired by the theoretical work of Haldenwang et al. [24]. A flow in two-dimensional channel was considered. At the channel walls, a constant fluid velocity in the wall-normal direction was imposed, U_0 which represents the permeation velocity. A parabolic velocity profile in the streamwise direction was imposed at the channel inlet. A specie (called 'A' for instance) was injected uniformly at the channel inlet, C_{in} , which value was maintained constant in time. The dimensionless Reynolds and Peclet of those simulations were $Re_0 = 0.758$ and $Pe_0 = 0.5$ both being based on U_0 for the velocity scale and H for the length scale. The time step was $dt = 10^{-3}H/U$ and the mesh size was The concentration profile C/C_{in} is plotted as a function of the wall-normal coordinate in figure 14,

at a distance $L/H = 10$ from the channel inlet. This figure shows a good agreement between the numerical solution and the theoretical prediction of [24].

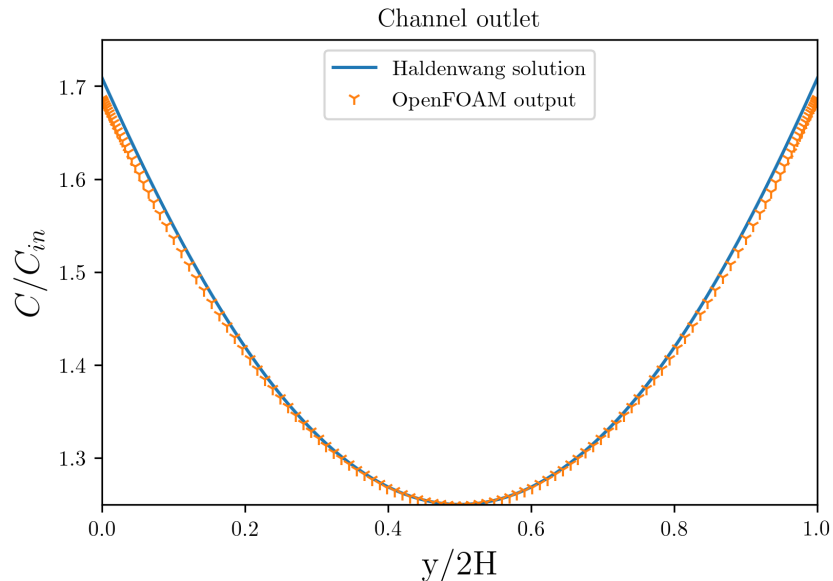


Figure 14: Comparison of the concentration profile obtained from OpenFOAM simulations (symbols) and the theory of [24] (solid line).

8.2 SI2 : Writing of equations in OpenFOAM formalism

OpenFOAM need a specific formalism for the equation writing. For instance, equation 7 is written whose solution is in OpenFOAM : `solve(fvm :: laplacian(p) == 16.0 * nu * rho * Lp/Foam :: pow(scd, 3.0) * (p - Pi/rho))`

8.3 SI3 : Additional contour for the relaxation after a filtration

The next figure represents the contour for the concentration during the relaxation after a filtration of a dispersion with a volume fraction of $\phi_0 = 0.02$ and $\phi_0 = 0.03$ $\phi_0 = 0.04$. To be complementary to the one presented in the article (Fig. 4 and 5), the color map is here at full scale for all contours (the maximum of the scale is then variable) to have a better visualization of the concentration profile.

The figure 14 for $\phi_0 = 0.3$ is the intermediate case between the Figure 4 and 5 presented in the paper. In these conditions the plugging by the gel appears only after a long time and it occupies a small part of the total volume (green line in the Fig. 7). It illustrates the transition from no plugging conditions with gel removal (Fig. 14) to conditions with gel plugging only at the end of the hollow fiber (Fig. 15) or over a significant length (Fig. 16).

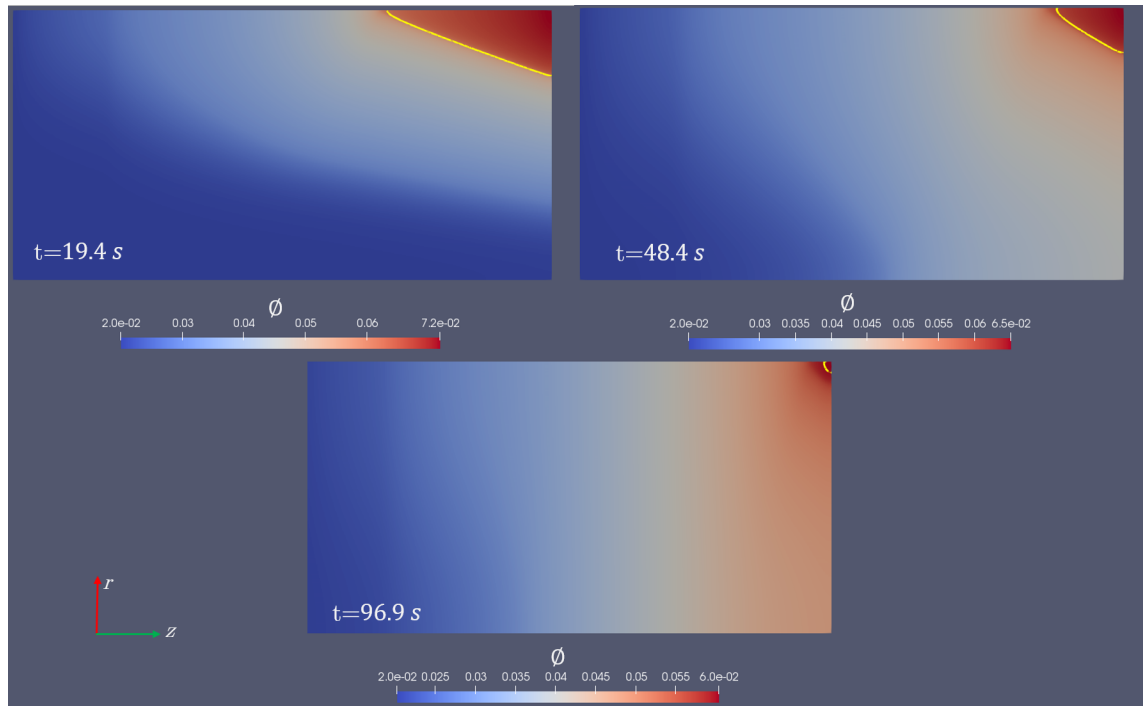


Figure 15: Contour plot of the concentrated layers inside the fiber for an injected concentration of $\phi_0 = 2 \times 10^{-2}$ after accumulation ($t = 0$) and during the relaxation times of 4.8, 9.7, 19.4, 48.4, 96.9, 193.7, 290.6, and 387.5 seconds. The fiber length is scaled by a factor 1/20 in the r -direction to ease the illustration of the concentration field. In each snapshot, the boundaries of each contour plot represent the membrane (top), the fiber center (bottom) the fiber inlet (left), and the fiber outlet (right). The yellow line denotes the limit of the gel phase, where the concentration is larger than $\phi_c = 0.06$.

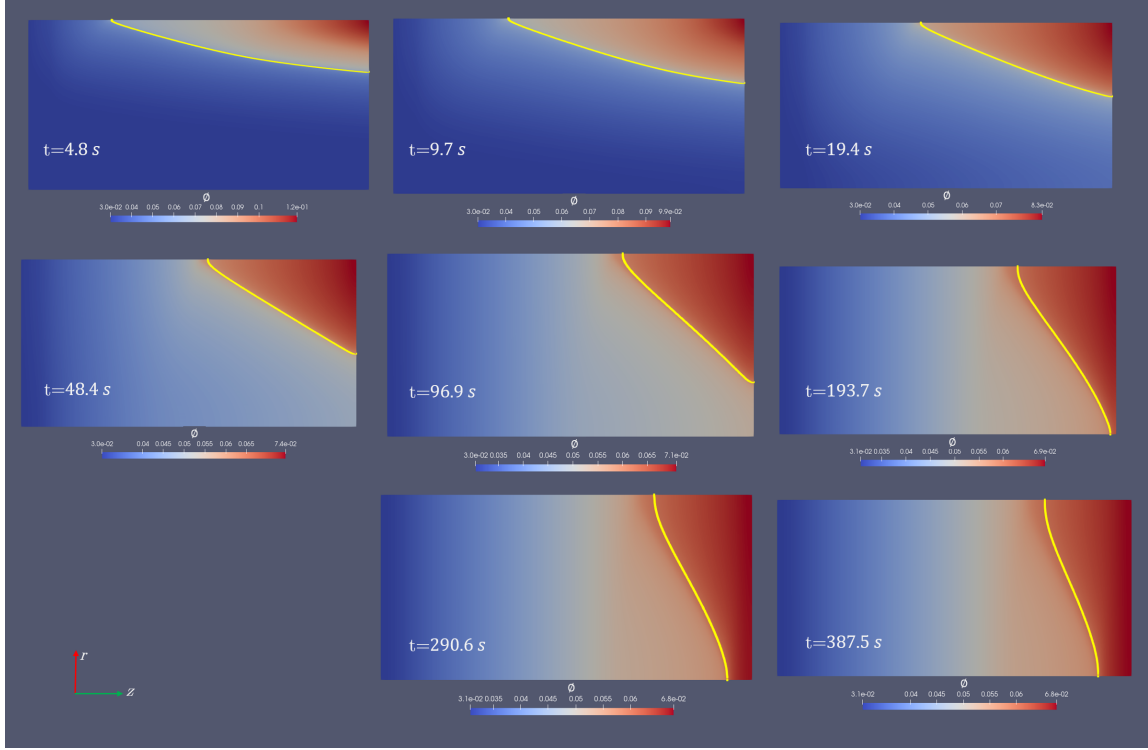


Figure 16: Contour plot of the concentrated layers inside the fiber for an injected concentration of $\phi_0 = 3 \times 10^{-2}$ after accumulation ($t = 0$) and during the relaxation times of 4.8, 9.7, 19.4, 48.4, 96.9, 193.7, 290.6, and 387.5 seconds. The fiber length is scaled by a factor 1/20 in the r-direction to ease the illustration of the concentration field. In each snapshot, the boundaries of each contour plot represent the membrane (top), the fiber center (bottom) the fiber inlet (left), and the fiber outlet (right). The yellow line denotes the limit of the gel phase, where the concentration is larger than $\phi_c = 0.06$.

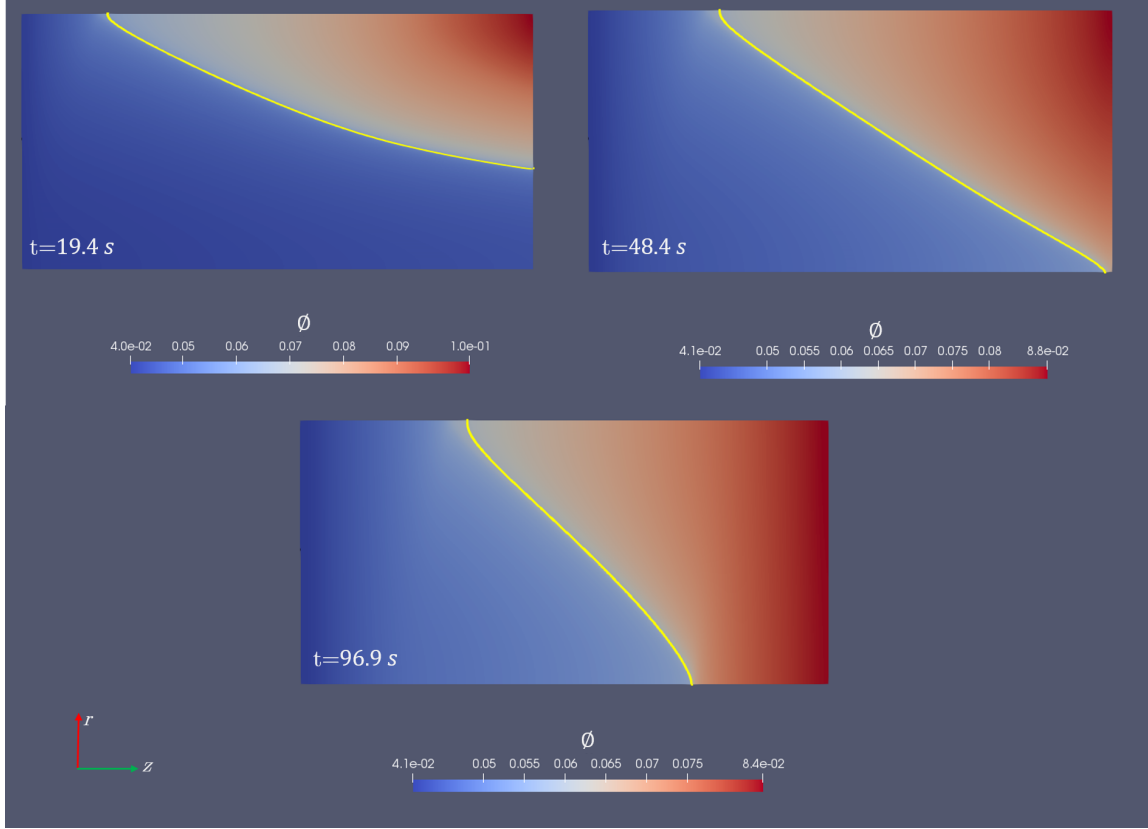


Figure 17: Contour plot of the concentrated layers inside the fiber for an injected concentration of $\phi_0 = 4 \times 10^{-2}$ after accumulation ($t = 0$) and during the relaxation times of 4.8, 9.7, 19.4, 48.4, 96.9, 193.7, 290.6, and 387.5 seconds. The fiber length is scaled by a factor $1/20$ in the r -direction to ease the illustration of the concentration field. In each snapshot, the boundaries of each contour plot represent the membrane (top), the fiber center (bottom) the fiber inlet (left), and the fiber outlet (right). The yellow line denotes the limit of the gel phase, where the concentration is larger than $\phi_c = 0.06$.